

Model Predictive Control of an Active Ankle-Foot Orthosis with Non-Linear Actuation Constraints

Benjamin DeBoer^{*a}, Ali Hosseini^a, Carlos Rossa^b

^a*Faculty of Engineering and Applied Science, Ontario Tech University, Oshawa, ON, Canada*

^b*Department of Systems and Computer Engineering, Carleton University, Ottawa, ON, Canada*

Abstract

The goal of active ankle-foot orthoses (AAFO) is to assist the user in recreating a nominal gait motion. Previously proposed control systems for AAFOs have been reactive, with controllers based on the current tracking error. However, the optimal AAFO controller must ensure adequate trajectory tracking while minimizing the amount of assistance provided to the user. To this end, a model predictive controller (MPC) can be considered to determine the optimal control sequence for a given trajectory. The MPC minimizes the control effort, thereby determining the minimal assistance required for a user to regain a natural gait. This work outlines the formulation of a non-linear MPC for an AAFO and its combination with an extended state observer (ESO) for tracking of an AAFO.

In this work, a MPC controller is proposed for optimal control of an AAFO, a linear plant subject to non-linear actuation constraints. A novel method is expressed to determine the initial control horizon selection in combination with variable step Newton-based optimization to enable real-time implementation. The MPC control effort is then combined with the estimated disturbance from an ESO to accurately track the desired gait.

Simulations and experimental results prove the tracking capabilities of the proposed method. Compared to a tuned proportional-derivative controller, the simulated controller reduced the trajectory tracking error by up to 65.1% and 15.3% in an undisturbed and disturbed environment, respectively. The MPC and ESO combination allows the controller to identify the optimal control action for accurate trajectory tracking. Concurrently, the ESO rejects both external and internal disturbances, with superior tracking capabilities in both undisturbed and heavily disturbed systems, making it the optimal choice for AAFO control.

Keywords: Non-Linear Model Predictive Control, Active Disturbance Rejection, Active Ankle-Foot Orthosis

*Email: benjamin.deboer1@ontariotechu.net, rossa@sce.carleton.ca.

SayedAli.Hosseini@ontariotechu.ca;

*Corresponding author: B. DeBoer.

Conflict of interest - none declared.

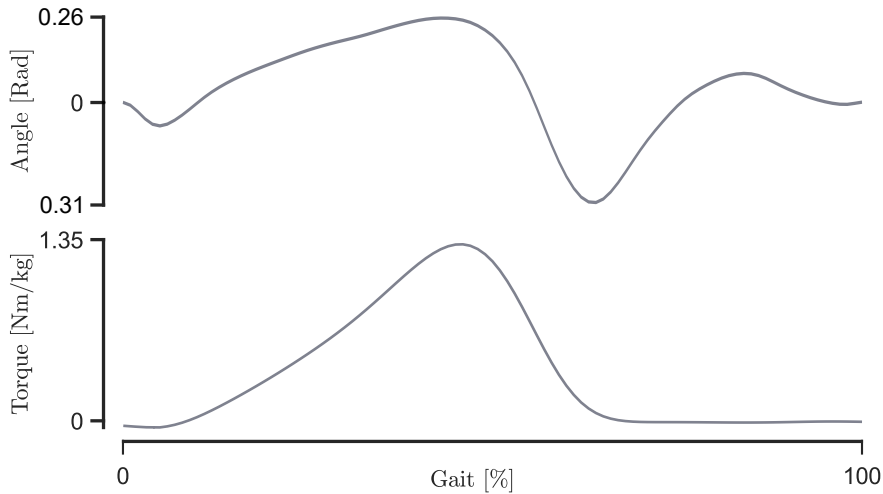


Figure 1: Nominal gait angular and torque trajectories. The torque of the ankle joint is dependent on the mass of the user. Data from [4].

1. Introduction

An active ankle-foot orthosis (AAFO) is an assistive device used to mechanically compensate for the effects of foot drop. A stroke can result in the onset of foot drop, in which the dorsiflexion ability of the anterior tibialis is unable to apply 60% of the nominal dorsiflexion torque [1]. Consequently, additional knee and hip flexions are induced to increase toe clearance, known as the steppage gait [2, 3]. AAFOs are designed to apply an assistive torque to the ankle joint to aid dorsiflexion and plantarflexion, reducing the effects of foot drop. The optimal AAFO aids the user in regaining a nominal gait cycle while applying the least amount of assistance. Therefore, impedance and model-based controllers have been proposed to minimize the tracking error between the AAFO and a nominal gait trajectory, shown in Fig. 1.

Impedance control was the first method implemented in an AAFO, where a series elastic actuator provided a force proportional to the position tracking error [5]. The controller separated the gait cycle into three phases. During the *heel contact to flat foot phase*, the controller applied impedance to resist plantarflexion; in the *stance phase*, no impedance is present; and during the *swing phase*, variable impedance is provided to ensure toe clearance. Other implementations of impedance control use a two-phase controller with a magnetorheological brake [6].

Model-based control, such as adaptive backstepping control [7], and slide mode control (SMC) [8], have been implemented widely in AAFOs. An extended state observer (ESO) added to SMC reduced the chattering effect of a large switching gain in the presence of large unmodelled disturbances and modelling errors [8], negatively affecting trajectory tracking controllers. Other methods have created adaptive controllers, introducing scaling constants to match the disturbance to a predefined model [2], along with efforts to reduce dynamic modelling errors [9]. The human gait is a slow process, with a total step time of 1.1 s as the average walking speed [4]. The goal of an ideal AAFO control system is to provide the least

required amount of assistance to achieve a nominal gait, making model predictive control (MPC) particularly advantageous.

The ankle joint during locomotion is subjected to a large plantarflexion torque disturbance, thus, the plant will not always react as the controller expects. MPC is advantageous for AAFO control in two ways: First, MPC incorporates the magnitude of the control effort when determining the optimal control action, minimizing the assistance to the user and reducing the opportunity for neuromuscular slaking while still achieving the desired trajectory [10]. Second, the control method and its resulting control values are based on the future trajectory allowing the controller to prepare for large acceleration instances, which is present multiple times within the gait cycle.

MPC has not yet been implemented for an AAFO. The closest implementations are Wang *et al.* [11], which proposed an end-point MPC controller to control the input to the hip and knee joints of the LOPES exoskeleton in the swing phase. Zarandi *et al.* [12] designed and implemented a non-linear MPC for the hip and knee joint using the active set method and time varying linearization, with constraints on the maximum torque output. To target the effects of foot drop, non-linear MPC has been used to control functional electrical stimulation [3]. The controller minimized the stimulus to the tibialis anterior to achieve a desired ankle angle in the swing phase. Other works have developed offline MPC controllers, in which the controller estimates the plant model and calculates two gains to be sent to a low-level controller operating in real-time [13]. Recently, Jammeli *et al.* implemented an explicit MPC combined with a non-linear disturbance observer for an actuated knee-joint orthosis [14]. The MPC was pre-solved offline to allow real-time implementation of the constrained cost function. The proposed architecture reduced the trajectory tracking error and minimized the assistance required from the user, all while requiring a similar torque magnitude as the compared proportional-integral-derivative controller [14].

This paper proposes a non-linear MPC framework that, when combined with an ESO, can achieve accurate trajectory tracking of an AAFO at varying levels of disturbance. The MPC controller relies on a linear plant model and a quadratic cost function containing the tracking error between the desired and actual plant trajectory, the magnitude of the control input, and a non-linear penalty function based on the output capability of the implemented actuator. To ensure quick convergence of the MPC cost function, a novel method to select an appropriate initial control sequence is proposed based on time-invariant acceleration of a linear system within a small timestamp. Newton-based optimization quickly minimizes the objective function at a low computational cost. An ESO is implemented to identify and reject any disturbance encountered by the plant. The ESO can reject both external and internal disturbances due to errors in the plant modelling. Simulations and experiments with an AAFO are conducted. The result is a controller with the ability to reduce the tracking error compared to a proportional-derivative (PD) controller.

This work presents a novel method of initial control horizon population and optimization, along with the contribution of a MPC and ESO combination for trajectory tracking of an AAFO. The paper is structured as follows: Section 2 describes the non-linear MPC formulation and optimization, followed by the simulation of the proposed controller and baseline PD controller in Section 3. Physical experiments are performed in Section 4, followed by

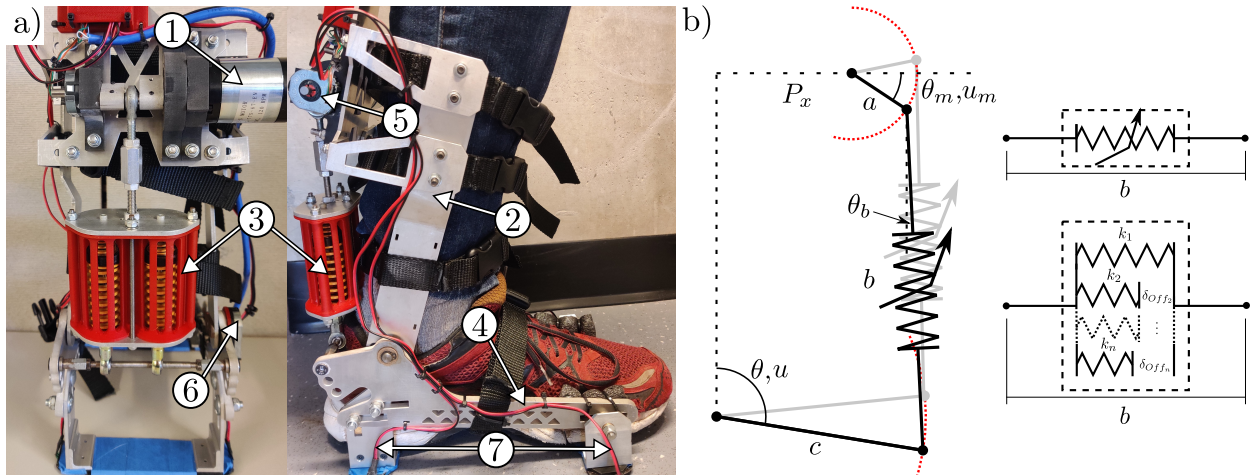


Figure 2: a) AAFO prototype powered by a DC motor and gearbox ① mounted to the shank ② and driving elastic element ③ to provide torque to the ankle joint, via the foot-bed ④. Two quadrature encoders are mounted to measure the DC motor ⑤ and ankle ⑥ rotation, and force sensitive resistors ⑦ are placed under the heel and toe to determine the current gait phase. b) The DN-SEA proposed in [15] encompassing a crank-rocker four-bar mechanism with a discrete non-linear link b .

the discussion of the proposed controller in Section 5. Conclusions and future work are presented in Section 6.

2. Non-Linear Model Predictive Control of an AAFO

The objective of MPC is to identify the optimal control sequence for a set number of discrete time steps, known as the control horizon, to minimize a cost function within another time interval, termed the prediction horizon. In the case of trajectory tracking, the cost function contains the tracking error and the magnitude of the control effort. Following the cost function optimization, the control sequence for the first discrete time step of the control horizon is applied to the plant. In linear MPC, the minimum of the objective function can be found by using quadratic programming, leading to the linear quadratic regulator in the unconstrained case [16]. However, linear MPC controllers with constraints require iterative computation using the Lagrangian algorithm, Karush-Kuhn-Tucker conditions, and other methods [16]. These methods are computationally expensive and hard to implement in real-time. Therefore, fast MPC methods have been developed in which the MPC controller computes only one optimization step per discrete time step in the control horizon [17]. In non-linear MPC, iterative optimization is required to minimize the cost function. Due to the high computational cost required to solve the cost function, non-linear MPC is implemented as suboptimal MPC, an alternative to optimal MPC in most cases [18].

The non-linear MPC presented here is based on a linear plant model with a non-linear torque constraint. The constraint is based on the geared direct current (DC) motor of the discrete non-linear series elastic actuator (DN-SEA), which should remain within the motors recommended range of operation. The AAFO being controlled is presented in Fig. 2a, with the discrete non-linear element shown in Fig. 2b. The device is free to rotate in the sagittal

plane, using the DN-SEA to provide the required assistive torque to the ankle joint [15]. The plant model is described as:

$$J\ddot{\theta}_a + B\dot{\theta}_a + K\theta_a = u - u_d \quad (1)$$

with state space representation:

$$\begin{bmatrix} \dot{\theta}_1 \\ \dot{\theta}_2 \end{bmatrix} = \begin{bmatrix} 0 & 1 \\ -\frac{B}{J} & -\frac{K}{J} \end{bmatrix} \begin{bmatrix} \theta_1 \\ \theta_2 \end{bmatrix} + \begin{bmatrix} 0 \\ \frac{1}{J} \end{bmatrix} (u - u_d) \quad (2)$$

where $\theta_1 = \theta_a$ and $\theta_2 = \dot{\theta}_a$, J is the rotational inertia, B is the damping coefficient, K is the stiffness of the AAFO at the ankle joint, and θ_a , $\dot{\theta}_a$, and $\ddot{\theta}_a$ are the angular position, velocity, and acceleration about the ankle joint, respectively. Control variables u and u_d are the MPC and ESO's control action and disturbance estimation, respectively. The proposed control topology is shown in Fig. 3. The ESO estimates the disturbance acting on the AAFO, pertaining to external or internal disturbance, such as the torque for locomotion or an error in plant modelling. The inverse of the estimated disturbance is added to the control signal to aid the MPC. The ESO is described in [9] as:

$$\begin{cases} \dot{\hat{\theta}}_1 = \hat{\theta}_2 + \beta_1 \text{fal}(e, \alpha_1, \delta) \\ \dot{\hat{\theta}}_2 = \hat{\theta}_3 + \frac{u - u_d - B\hat{\theta}_2}{J} + \beta_2 \text{fal}(e, \alpha_2, \delta), \quad \text{where } u_d = J\hat{\theta}_3 \\ \dot{\hat{\theta}}_3 = \beta_3 \text{fal}(e, \alpha_3, \delta) \end{cases} \quad (3)$$

where $\hat{\theta}_1$, $\hat{\theta}_2$, $\hat{\theta}_3$ are the observed states of θ_a , $\dot{\theta}_a$, $\ddot{\theta}_a$, the observed error is $e = \theta_a - \hat{\theta}_1$, $\alpha_1 = 3 \cdot 10^2$, $\alpha_2 = 3 \cdot 10^4$, $\alpha_3 = 1 \cdot 10^6$, $\delta = 0.001$, and $\text{fal}(e, \alpha, \delta)$ is the non-linear gain function defined as [19]:

$$\text{fal}(e, \alpha, \delta) = \begin{cases} \frac{e}{\delta^{1-\alpha}}, & |e| \leq \delta \\ |e|^\alpha \text{sign}(e), & |e| \geq \delta \end{cases} \quad (4)$$

The scalar values β_1 , β_2 , and β_3 are determined by manual pole placement at -100 as described in [9], inspired by the work in [20]. The MPC controller has three main components: (1) The cost function determines the controller response to the desired input based on its architecture and weighting matrices, (2) the method of initial control horizon selection, and (3) subsequent optimization allows the sub-optimal control sequence to be identified within a short time.

2.1. Cost Function

The AAFO's cost function tracks the desired trajectory, while minimizing the assistance provided by the AAFO, all while abiding by the system constraints. The proposed AAFO has a non-linear constraint, with the applied torque of the DC motor and the torque transmitted to the ankle joint having a non-linear relationship. The constraint corresponds to

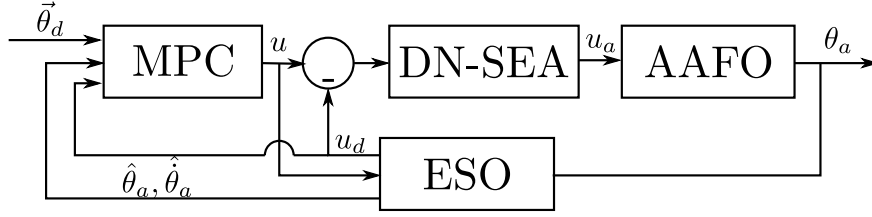


Figure 3: The proposed control system combining the MPC controller and an ESO. The MPC controller is provided with the desired trajectory ($\vec{\theta}_d$), the plant's estimated angular position and speed ($\hat{\theta}_a, \hat{\theta}_a$), and the estimated disturbance torque u_d . The MPC control provides the optimal control torque u to the DN-SEA and ESO. The actuator applied torque u_a ($u_a = u - u_d$ in the ideal case) is applied to the AAFO plant which determines the ankle position and feeds it to the ESO.

the maximum recommended torque of the motor and gearbox. The inequality constraint is applied as a penalty function in a basic MPC quadratic cost function, expressed as:

$$C(\vec{u}, u_d) = \underbrace{\left\| \vec{\theta}_d - \vec{\theta}_a \right\|_Q^2}_{\text{Trajectory}} + \underbrace{\left\| \vec{u} \right\|_R^2}_{\text{Control}} + \underbrace{\left\| C_a(u_m(\vec{u}, u_d, \vec{\theta}_a)) \right\|_S^2}_{\text{Penalty Function}} \quad (5)$$

with:

$$\vec{\theta}_d = [\theta_{d_1} \dots \theta_{d_N}], \quad \vec{\theta}_a = [\theta_{a_1} \dots \theta_{a_N}], \quad \vec{u} = [u_1 \dots u_M]$$

where Q , R , and S are positive definite weighting matrices, $\vec{\theta}_d$ and $\vec{\theta}_a$ are the desired trajectory and estimated plant output for a fixed prediction horizon of length N ; \vec{u} is the required torque at the ankle for a fixed control horizon of length M , where $M \leq N$. If $M < N$, the last value in the control horizon is used for the remainder of the prediction horizon. The weighting matrix Q is linearly decreasing, such that trajectory tracking errors early in the prediction horizon significantly affect the cost function. The opposite is true for the R and S matrices, with a linearly increasing weight within the matrices. The linearly increasing and decreasing weighting matrices result in a cost function that minimizes trajectory tracking in the immediate prediction horizon, while minimizing the applied assistance at the end of the control horizon. Function C_a is a quadratic penalty forcing the applied motor torque to remain within the recommended operating range ($[-u_{m_{max}} \ u_{m_{max}}]$) of the motor and gearbox, defined as:

$$C_a(u_m(u, u_d, \theta)) = \begin{cases} (|u_m(u, u_d, \theta)| - u_{m_{max}})^2, & |u_m(u, u_d, \theta)| > u_{m_{max}} \\ 0, & \text{Otherwise} \end{cases} \quad (6)$$

and $u_m(u, u_d, \theta)$ is determined by [15]:

$$u_m(u, u_d, \theta) = (u - u_d) \left(\frac{a \cos(\theta_m - \theta_b)}{c \sin(\theta - \theta_b)} \right) \quad (7)$$

where a and c are link lengths of the DN-SEA, θ_b is the absolute angle of link b with respect to the origin, and θ_m is the motor's position, see Fig. 2b. The parameters and formulations

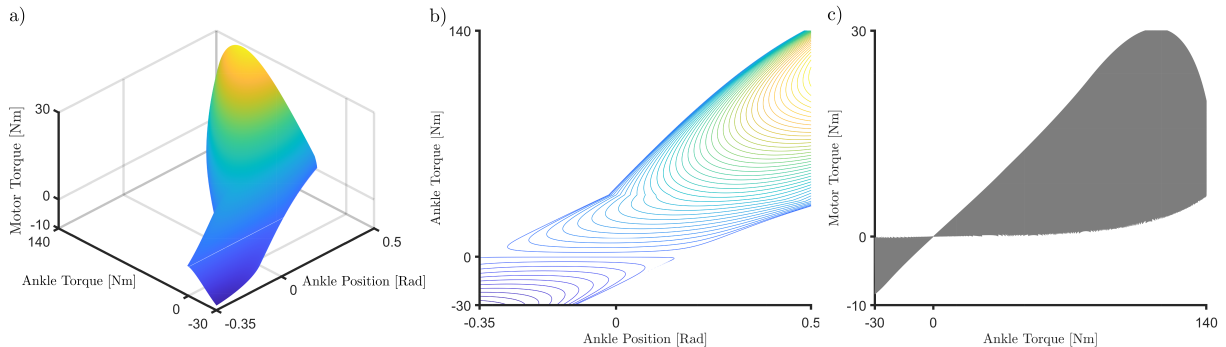


Figure 4: Ankle and motor torque relationship of the DN-SEA under varied ankle position. The nonlinear relationship between the ankle and motor torque is shown in the surface plot a) in conjunction with the contour plot b) and torque comparison plot c). It is clear that the relationship between the torque at the ankle and motor are dependent on the position of the ankle.

are further described in [15]. The maximum applied torque at the ankle joint varies depending on θ , creating the non-linearity depicted in Fig. 4. The implementation of a penalty function is used instead of a hard constraint, as the motor and gearbox combination can achieve torque above the recommended operation limit, however, instances of high torque should be minimized. The penalty function does not guarantee constraint adherence but instead encourages the motor torque to remain within the recommended range of operation. Additionally, the unconstrained optimization problem is significantly faster to compute. The proposed cost function targets the minimization of the trajectory tracking error, magnitude of the control effort, while encouraging the applied motor torque to remain within an acceptable limit. With the plant and cost function defined, the minimization of the objective function can be achieved using various methods. However, to reach real-time operation, non-linear MPC requires an initial estimate of a control horizon in close proximity to a local minimum.

2.2. Initial Population of the Control Horizon

Given the desired angular trajectory ($\vec{\theta}_d$), the time discretization (Δt), and control (M) and prediction (N) horizon lengths, the initial values of the control horizon (\vec{u}) can be determined by assuming invariant acceleration. In the case Δt is sufficiently small, the desired acceleration ($\ddot{\theta}_d$) at each point in the control horizon is determined by:

$$\ddot{\theta}_d(i) = \frac{2 \left(\theta_d(i) - \theta_s - \dot{\theta}_s \Delta t \right)}{\Delta t^2}, \forall i \in [1, M] \quad (8)$$

where $\theta_d(i)$ is the desired position at prediction horizon index i , and θ_s and $\dot{\theta}_s$ are the simulated position and velocity of the plant, equal to $\theta_s = \hat{\theta}_a$ and $\dot{\theta}_s = \hat{\dot{\theta}}_a$, when $i = 1$. The ESO is critical as it provides a sufficient observation of $\dot{\theta}_a$ required for initialization. The desired rotational acceleration is translated to the estimated control torque (u_e), using the

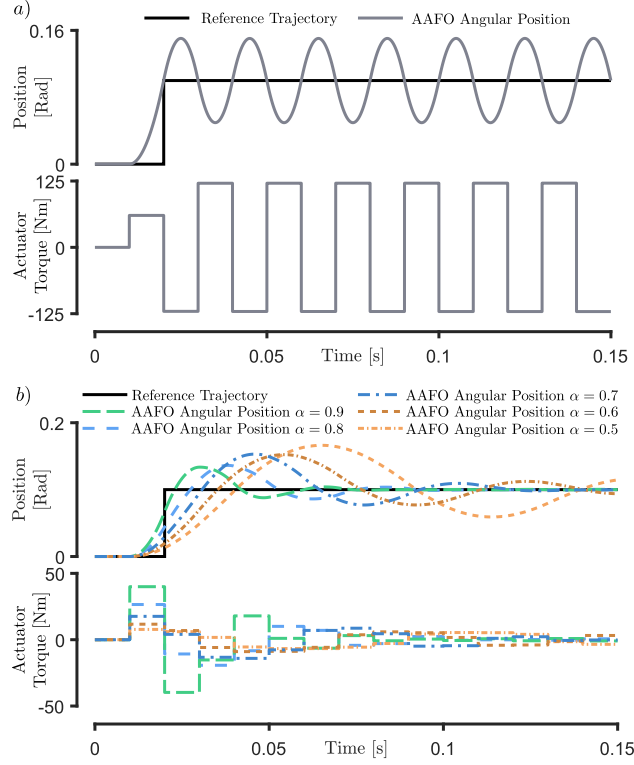


Figure 5: a) Linear approximation control in response to a step input of 0.1 rad at $t = 0.02$ s. b) Result of linear approximation control with varying saturation gains (α).

average speed and position:

$$u_e(i) = J\ddot{\theta}_d(i) + B \left(\frac{\dot{\theta}_d(i) + \dot{\theta}_s}{2} \right) + K \left(\frac{\theta_d(i) + \theta_s}{2} \right) \quad (9)$$

with:

$$\dot{\theta}_d(i) = \dot{\theta}_s + \ddot{\theta}_d(i)\Delta t.$$

The plant is then simulated with control $u_e(i)$ for time Δt to determine the simulated plant's position (θ_s) and velocity ($\dot{\theta}_s$). The remainder of the control horizon (M) is then incrementally determined using the position determined at the last time stamp and the desired position at the next time stamp ($\theta_d(i)$). If $M < N$, the last control horizon value ($u_e(M)$) is determined using the last position of the prediction horizon $\theta_d(N)$.

The control horizon is initially tested in response to a step input, see Fig. 5a. The response is marginally stable and is not a suitable initial control sequence. Therefore, to reduce the chattering control signal presented, the non-linear gain function with $\delta = 0$ and $e = u_e(i)$ is used, modifying (4) to:

$$fal(u_e(i), \alpha) = |u_e(i)|^\alpha \text{sign}(u_e(i)). \quad (10)$$

This modified function dampens the determined control input, where $\alpha \in [0, 1]$ is the saturation gain, and $i \in [1, M]$ is the index of \vec{u}_e . Eq. (10) is implemented before the simulation

of time Δt during each time step of the initialization. Implementing (10) results in a stable response to a step input when $\alpha < 1$, see Fig. 5b. The proposed control initialization method provides a sufficient initial guess for the MPC controller, where tuning parameter α can be adjusted to place the optimizer in the region of the desired response.

2.3. Optimization

The cost function can now be minimized using Newton-based methods, starting at the initial guess. The optimization is unconstrained, allowing the controller to focus on assisting the user while minimizing the risk of the controller applying a stiff control correction if a user violates a constraint. The Gauss-Newton optimizer is commonly used to minimize least-squared objective functions, where the algorithm targets the closest minima/maxima to the initial guess. Due to the non-linearity imposed by the penalty function, the Newton-Raphson approach can be used before exploring the minima using Gauss-Newton. The Newton-Raphson method aims to identify a root of a given function, with the update term $\frac{f(x)}{f'(x)}$, to target the position of a local minimum in the objective space. Multi-variate Newton-Raphson updates the decision variables via:

$$\vec{u}_{k+1} = \vec{u}_k + \underbrace{\gamma L_k^{-1} c_k}_{\text{Update Term}} \quad (11)$$

where u_k is the optimized control vector, initially $u_k = u_e$, k is the previous iteration, c_k is the cost at iteration k , L is the Jacobian matrix, and γ is the Newton step scaling factor. When the Newton-Raphson method approaches a local minimum, the magnitude of the update term increases, reducing the ability of the optimizer to determine the best control sequence in the minima. To closely identify the local minima, Gauss-Newton method is then evaluated to find the absolute minima, with an update term of $\frac{f'(x)f(x)}{f''(x)}$, expressed as:

$$\vec{u}_{k+1} = \vec{u}_k + \underbrace{\gamma (L_k L_k^T + \lambda I)^{-1} L_k c_k}_{\text{Update Term}} \quad (12)$$

where $L_k L_k^T$ is an approximation of the Hessian matrix, and I is an identity matrix combined with a small scalar λ to ensure matrix inversion.

The step size γ can also be varied to increase performance. In this work, the search method from the fast jaguar algorithm is adapted [21]. Once an instance of a minimum is identified and the following iteration results in a worse objective function value, the variable step method is implemented, where the new step scalar is updated as:

$$\gamma = \begin{cases} 2\gamma, & \text{if } C_{k+1} < C_k \\ 1, & \text{if } \gamma > 1 \\ \frac{\gamma}{2}, & \text{Otherwise} \end{cases} \quad (13)$$

in which C_{k+1} and C_k is the result of the objective function at the current and previous iteration, and γ is limited to ≤ 1 . The complete optimization flow is presented in Fig. 6,

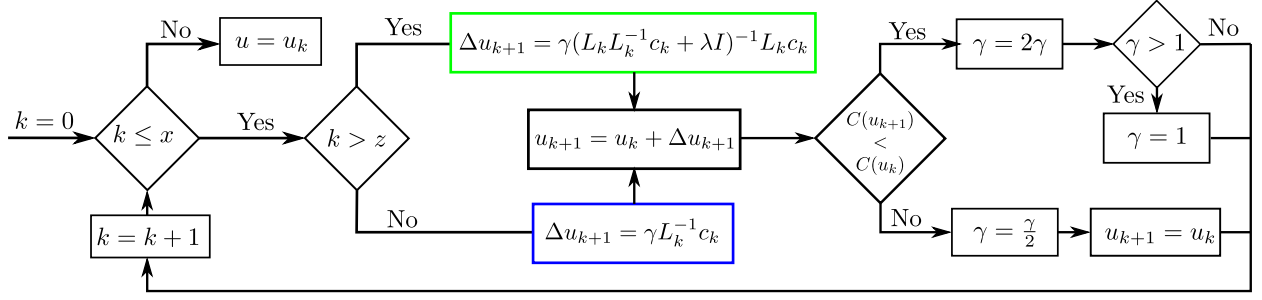


Figure 6: MPC optimization method, in which the Newton-Raphson algorithm (blue) is implemented z times followed by $z - x$ Gauss-Newton (green) iterations, where x and k are the total number and current iteration, respectively.

where x , z , and k are the total number of iterations, number of Newton-Raphson iterations, and current iteration, respectively. To clarify, the Jacobian used for the Newton-based optimization is determined iteratively, as the derivative of the cost function described in (5) can not be determined analytically. At each iteration, the Jacobian is determined by:

$$L_k = \frac{c_k - c_{k-1}}{\vec{u}_k - \vec{u}_{k-1}}. \quad (14)$$

To initialize the Jacobian from the initial guess, the cost and control of the initial guess are denoted c_k and \vec{u}_k . The initial guess is then shifted by a scaling factor ($\vec{u}_{k-1} = \vec{u}_k(1 + \eta)$), where η is sufficiently small.

3. Simulation Results

Simulations are conducted to analyze the benefits and restrictions of the proposed controller in conjunction with an ESO. The MPC controller is initialized with a control and prediction horizon of $M = 3$ and $N = 5$, operating at 100 Hz with the 200 Hz ESO presented in [9]. To minimize the objective function, the optimization method is set to conduct 50 iterations ($x = 50$), starting with two Newton-Raphson iterations ($z = 2$), with cost function matrices Q , R , and S having weights of 10, 10^{-4} , and 1, respectively, resulting in weighting matrices of:

$$Q = \begin{bmatrix} 10 & 0 & 0 & 0 & 0 \\ 0 & 8.13 & 0 & 0 & 0 \\ 0 & 0 & 6.25 & 0 & 0 \\ 0 & 0 & 0 & 4.38 & 0 \\ 0 & 0 & 0 & 0 & 2.50 \end{bmatrix}, R = \begin{bmatrix} 6.25e^{-5} & 0 & 0 \\ 0 & 8.13e^{-5} & 0 \\ 0 & 0 & 10.0e^{-5} \end{bmatrix}, S = \begin{bmatrix} 0.63 & 0 & 0 \\ 0 & 0.81 & 0 \\ 0 & 0 & 1 \end{bmatrix}.$$

The low control weight R is based on the high torque required by the ankle joint and its low angular range. Fig. 1 shows that the ankle has a range of only 0.57 radians, where the torque output of the ankle joint reached 1.35 Nm per kg of the user's mass. To find the ideal saturation gain for the initial control horizon, the plant is exposed to a ramp input with

$\alpha \in [0, 1]$. A saturation gain of $\alpha = 0.65$ was selected from the objective function minima as α is varied. For a MPC comparator, a discrete PD controller with a sampling rate of 1 kHz is implemented, tuned to achieve a 0.063s settling time when exposed to a 0.1 rad step input. The ESO is combined with the PD control to create an accurate comparison. The PD controller is given a proportional and derivative gain of 200 and 4, respectively. The result of the MPC and PD tunings are 127 ms and 54 ms settling times, respectively. The gait trajectory from [4] is used as the desired angular trajectory of the ankle joint and gait disturbance for the simulations.

Three types of simulations are conducted to compare the controllers i.e., with no disturbance, nominal gait disturbance, and sinusoidal disturbance. Since the plant parameters of the AAFO in combination with the foot cannot be measured, three variations of the plant model are simulated:

1. No Modelling Error: The MPC, ESO, and simulated plant have identical parameters.
2. Plant Modelling Error 1 (PME₁): The MPC and ESO are given the same plant parameters of the first variation, however, the simulated plant is given a 33% higher inertial value.
3. Plant Modelling Error 2 (PME₂): The MPC and ESO are given the same plant parameters of the first variation, however, the simulated plant is given 33% and 50% lower inertial and damping values, respectively.

The simulations were conducted with a gait speed of 1.1 s with a 3-step snapshot presented in Fig. 7 and 8, with the respective root mean square tracking error (RMSE) presented in Table 1. Large modelling discrepancies are used in this test as the combined inertial and damping parameters of the AAFO and foot can not be measured, leading to potentially large modelling errors in the controller’s model. The results show that the MPC and ESO combination is the best trajectory tracking controller, even in the presence of high amplitude gait and sinusoidal disturbance. The combination allows the MPC controller to focus on accurate trajectory tracking, while the ESO rejects any disturbance applied to the plant. Fig. 7c and 7d show the estimated disturbance lags behind the true disturbance, resulting in an increased trajectory tracking error when the disturbance torque changes. In Fig. 8a and d, it is evident that the ESO can identify and reject the disturbance due to the plant modelling error, where PME₁ and PME₂ result in opposing disturbance torques due to the large difference in rotational inertia. The trend is visible throughout Fig. 8, where the disturbance estimated with PME deviates from the induced disturbance. In the case of PME₂, the trajectory tracking error is best, as the simulated plant has a reduced inertial and damping parameter, resulting in a stiff and quick plant response. The MPC and ESO can handle external and internal disturbances while achieving better tracking performance compared to an ESO and PD controller tuned for a fast-settling time. The PD controller is only advantageous when compared to the MPC with no ESO, as the high gains of the PD controller compensate for the induced disturbance.

Table 1: RMSE Simulation Results for MPC and PD controller in combination with the ESO in the presence of gait and sinusoidal disturbance (10^{-3}).

Controller	No Disturbance	Gait Disturbance	Sinusoidal Disturbance
MPC	2.09	336	540
MPC+ESO	1.80	9.74	8.36
MPC+ESO PME ₁	3.29	11.0	9.30
MPC+ESO PME ₂	1.56	9.54	7.38
PD	5.20	142	166
PD+ESO	5.16	11.5	9.52
PD+ESO PME ₁	5.46	11.7	9.68
PD+ESO PME ₂	4.96	11.3	9.41

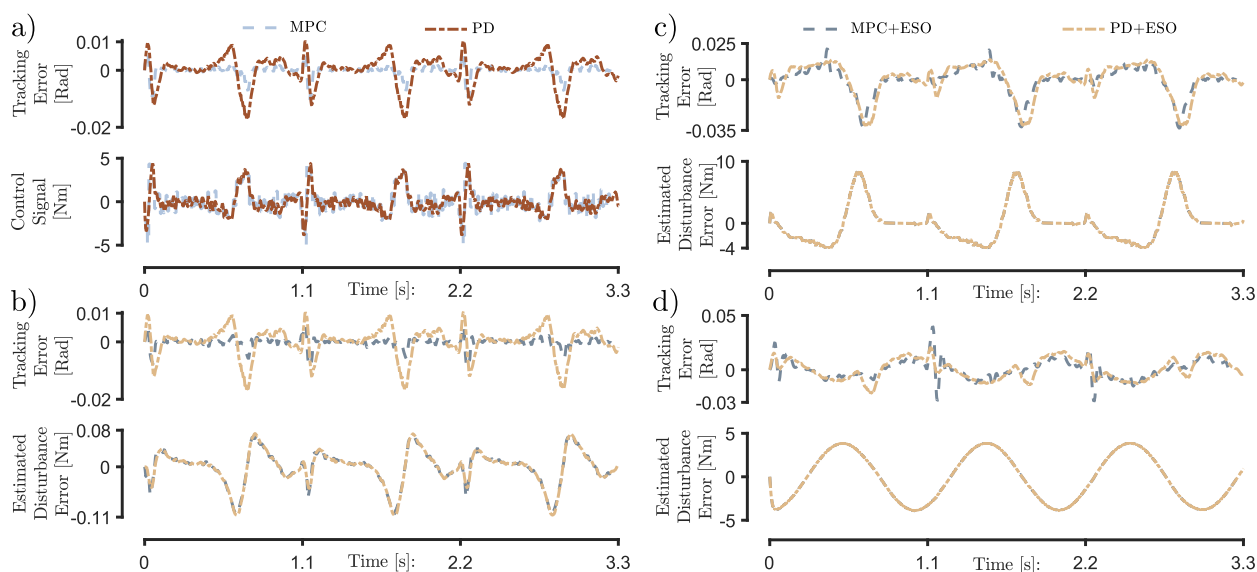


Figure 7: a) Simulation results of the standalone MPC and PD controller without disturbances, b) simulation results of the MPC and PD controller combined with the ESO, c) simulation results with gait disturbance for a 40 kg user and d) 1 Hz 40 Nm sinusoidal disturbances. Tracking errors are based on the actual and desired angular trajectory of the ankle joint, presented in Fig. 1. Estimated disturbance error is the difference between the measured and rejected disturbance by the ESO and the induced disturbance torque.

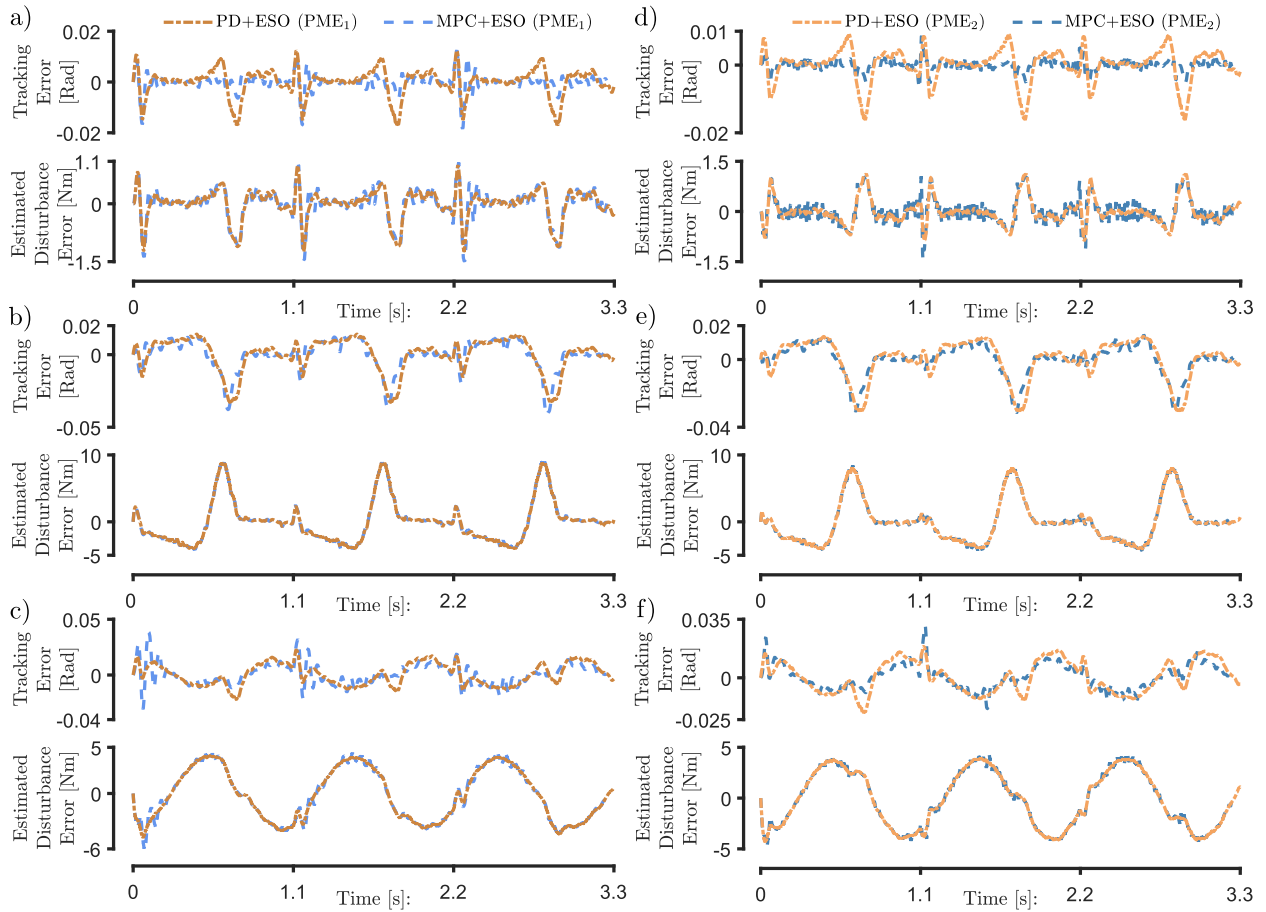


Figure 8: Simulation results of the MPC and PD controllers with the ESO in the presence of plant modelling error. a) and d) present the response without disturbances, b) and e) show the simulation results with gait disturbances for a 40 kg user and c) and f) present the simulation results for a 1 Hz 40 Nm sinusoidal disturbance, for PME_1 and PME_2 , respectively. Tracking errors are based on the actual and desired angular trajectory of the ankle joint, presented in Fig. 1. Estimated disturbance error is the difference between the measured and rejected disturbance by the ESO and the induced disturbance torque.

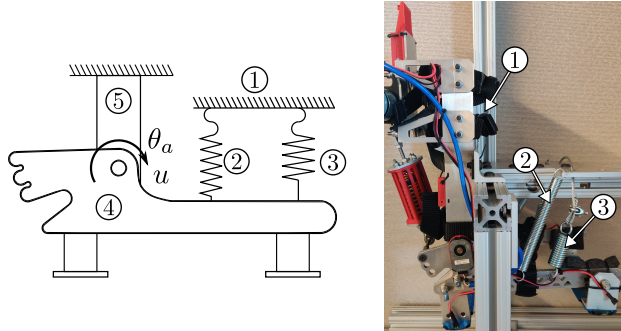


Figure 9: MPC experimental setup, with a rigid structure ① to fix the AAFO shank ⑤. Disturbance is created using unidirectional springs with a 3.0 N/mm ② and 13.9 N/mm ③ stiffness, connected between the test structure and foot bed ④. The springs are combined to create a low, medium, and high disturbance during plantarflexion.

4. Experimental Validation

An AAFO prototype is used to conduct trajectory tracking under varying load disturbances to validate the simulations. The AAFO, see Fig 9, is equipped with a DN-SEA, two quadrature encoders to measure the ankle and motor position, and two sets of force-sensitive resistors to synchronize the controller to the current user’s gait phase. The proposed control system is implemented in C++ on a Windows computer (Intel Core2 Quad 2.50 GHz, 6 Gb DDR2) with a data-acquisition card (Humusoft MF634). The program is structured into three threads: PD motor position control (20 kHz), data logging (100 Hz), and the main control loop, which executes the MPC controller at 100 Hz and the ESO at 200 Hz.

Two sets of experiments are conducted. In experiment 1, the AAFO is mounted on the test stand (See Fig. 9) and is free from external disturbances. For experiment 2, the AAFO remains in the test stand, where two sets of springs (experimentally measured to be 3.0 N/mm and 13.9 N/mm) are used individually, and in combination, to generate an unknown light, medium, and heavy disturbance (See Fig. 9), generating a peak torque of 16.7 Nm, 27.94 Nm, and 31.54 Nm, respectively. The MPC and PD controllers are set to track the nominal trajectory in 3.3 s. Fig. 10 shows the trajectory tracking results of the MPC+ESO and PD+ESO controllers for both experiments, and Table 2 displays the RMSE and average current. The mean, standard deviation, and maximum computation time for the MPC controller are 99.29 μ s, 70.66 μ s, and 396.9 μ s, respectively. In contrast, the same metrics for the PD controller are 0.34 μ s, 0.08 μ s, and 0.7 μ s, respectively. Similarly, the computation time of the ESO has a mean, standard deviation, and maximum of 42.8 μ s, 3.7 μ s, and 89.5 μ s, respectively in the MPC experiment and 46.5 μ s, 3.2 μ s, and 120 μ s, respectively for the PD experiment.

5. Results & Discussion

The simulation and experimental results show the feasibility and benefits of the proposed real-time MPC controller in combination with the ESO. The simulations prove that the proposed architecture has significant benefits, with an RMSE reduction of 58.3%, 12.3%, and

Table 2: Experimental Results

Disturbance	MPC+ESO	PD+ESO	MPC+ESO	PD+ESO
	Tracking Error RMSE (10^{-3})		Average Current [mA]	
No Dist.	89.4	70.6	484	467
Light Dist.	95.4	86.9	432	427
Medium Dist.	97.5	90.0	446	448
High Dist.	106.2	105.5	528	648

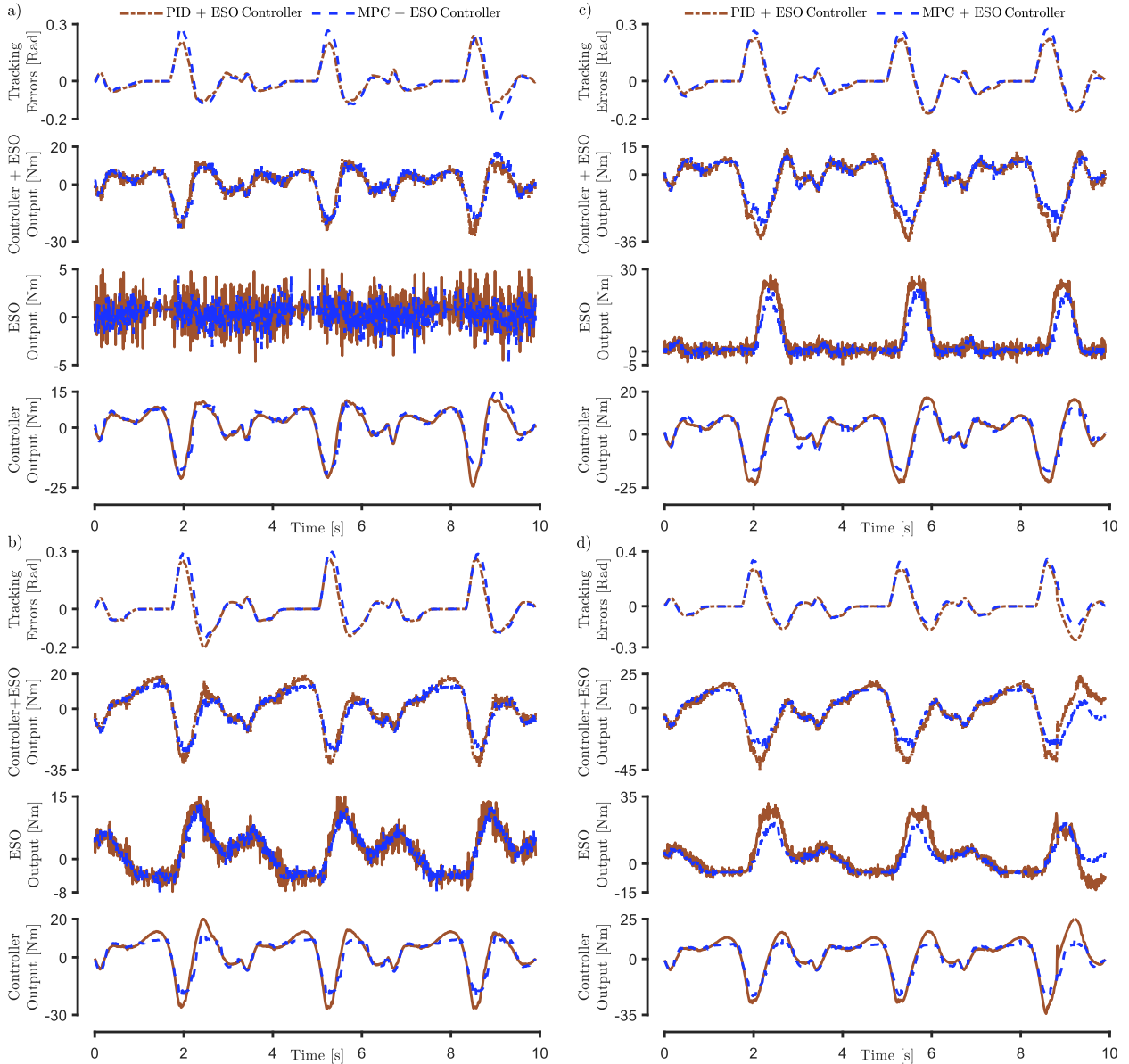


Figure 10: MPC and PD controller tracking without disturbance a) and in the presence of b) light disturbance, c) medium disturbance, and d) heavy disturbance.

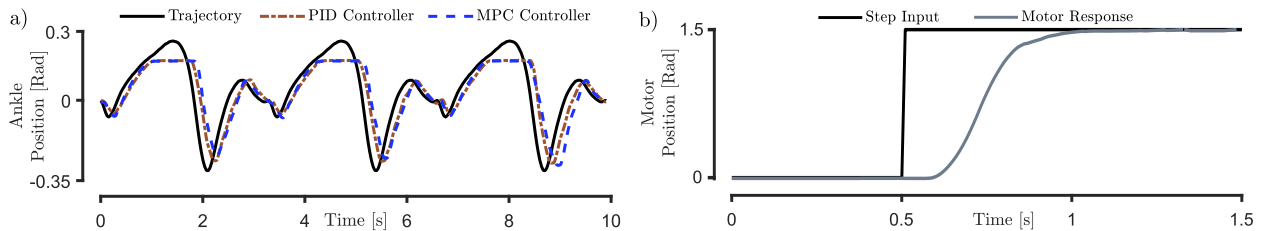


Figure 11: a) Physical testing desire and actual trajectories. The delay is caused by the employed DC motor and gearbox. The time delay and step input of the motor can be seen in b). It is noted that the physical limitations of the AAFO actuator in the presence of no disturbance restricts the dorsiflexion range of motion to 0.174 rad.

12.6% in the presence of no disturbance, nominal gait disturbance, and sinusoidal disturbance with respect to the PD and ESO combination. The method proposed to determine the initial control horizon effectively leads the MPC in sufficient trajectory tracking. However, the implementation of the ESO must be included to accurately track the nominal trajectory in the presence of high disturbance and errors in the plant model.

Experimental testing outlines two benefits of the MPC controller. First, the required torque from the MPC and ESO combination is reduced by 16.3% compared to the PD and ESO combination in the presence of high disturbances. Fig. 10 shows the proactive approach of the MPC controller reducing the control value in anticipation of the future trajectory. Table. 2 shows that the MPC and PD controller have similar tracking errors, with a reduced input current seen by the MPC during high disturbances. The results show that the MPC considers a balanced control approach instead of the high-gain PD controller. Second, the experiments show the real-time capability of the proposed controller. The combined maximum MPC and ESO computation time did not exceed $486.4 \mu\text{s}$, which is significantly less than the required cycle time of the ESO and MPC controller (5 and 10 ms, respectively).

Fig. 11, shows the trajectory tracking capability of the proposed real-time MPC and ESO and that of the PD and ESO controller. A significant contribution to the observed error is the presence of torque application delay. A delay is present between the MPC and PD controllers response and the desired trajectories (see Fig. 11a). The delay is a result of the activation time of the geared DC motor. Fig. 11b shows the motor's position response to a step input position. 90 ms elapses before motion is present at the end of the gearbox. The delay will be included in future plant models to reduce the tracking error. Consequently, the PD controller has increased trajectory tracking performance with an actuation delay, as the high tuning gains generate a substantial torque with the increased tracking error. The effect is also present in the case of the MPC and PD only controllers in Table. 1, due to the high tracking error. The proposed combination does outperform the PD controller in the physical testing at higher disturbances while minimizing the amount of energy used.

The MPC and ESO combination is an effective control strategy for AAFOs. The MPC controller targets accurate trajectory tracking with the conscious effort of minimizing the applied assistance to the user. The ESO identifies and rejects external and internal dis-

turbances to the system. In the future, the ESO could be seen as a dependency to the AAFO user, as the disturbance due to insufficient push-off torque from the users will be supplemented by the ESO. Therefore, limits can be applied to the ESO to allow only a certain percentage of the nominal ankle torque to be applied via the ESO. In the presence of increased muscle activation of the user during operation, the weight matrix R of the MPC cost function can be incremented, and the percentage of nominal ankle torque from the ESO can be decremented, until there is no longer assistance required for user locomotion.

6. Conclusion

This work presents a combined non-linear MPC and ESO for active ankle foot orthoses. The AAFO is considered a linear plant with non-linear constraints due to the actuator's non-linearities. Therefore, a non-linear MPC controller is developed to achieve accurate trajectory tracking, with an ESO to minimize the effect of gait disturbances and plant modelling errors. Simulation and physical tests show the tracking accuracy and real-time capability of the proposed control topology. The benefit of the MPC implementation is the inclusion of the control magnitude in the cost function, allowing the controller to minimize assistance to the user experiencing temporary or persisting foot-drop.

Future work will focus on testing the device with a motor of low latency and including the mechanical delay into the plant model. It is estimated that this will eliminate most of the error between the simulated and physical results. Finally, adaptive laws can be introduced into the controller, actively minimizing plant modelling errors.

References

- [1] A. E. Carolus, M. Becker, J. Cuny, et al., The interdisciplinary management of foot drop, *Deutsches Ärzteblatt International* 116 (20) (2019) 347.
- [2] V. Arnez-Paniagua, H. Rifai, Y. Amirat, et al., Adaptive control of an actuated ankle foot orthosis for paretic patients, *Control Engineering Practice* 90 (2019) 207–220.
- [3] M. Benoussaad, K. Mombaur, C. Azevedo-Coste, Nonlinear model predictive control of joint ankle by electrical stimulation for drop foot correction, in: *IEEE/RSJ International Conference on Intelligent Robots and Systems*, 2013, pp. 983–989.
- [4] G. Bovi, M. Rabuffetti, P. Mazzoleni, et al., A multiple-task gait analysis approach: kinematic, kinetic and emg reference data for healthy young and adult subjects, *Gait & posture* 33 (1) (2011) 6–13.
- [5] J. A. Blaya, H. Herr, Adaptive control of a variable-impedance ankle-foot orthosis to assist drop-foot gait, *IEEE Transactions on neural systems and rehabilitation engineering* 12 (1) (2004) 24–31.
- [6] D. Adiputra, A. Rahman, M. Azizi, et al., Control reference parameter for stance assistance using a passive controlled ankle foot orthosis—a preliminary study, *Applied Sciences* 9 (20) (2019) 4416.
- [7] O. Kirtas, Y. Savas, M. Bayraker, et al., Design, implementation, and evaluation of a backstepping control algorithm for an active ankle-foot orthosis, *Control Engineering Practice* 106 (2021) 104667.
- [8] J. Zhao, T. Yang, X. Sun, et al., Sliding mode control combined with extended state observer for an ankle exoskeleton driven by electrical motor, *Mechatronics* 76 (2021) 102554.
- [9] B. DeBoer, A. Hosseini, C. Rossa, An extended parameter estimation disturbance observer for an active ankle foot orthosis, in: *IEEE International Conference on Systems, Man, and Cybernetics (SMC)*, 2021, pp. 1105–1110. doi:10.1109/SMC52423.2021.9659241.
- [10] L. N. Awad, P. Kudzia, D. A. Revi, T. D. Ellis, C. J. Walsh, Walking faster and farther with a soft robotic exosuit: Implications for post-stroke gait assistance and rehabilitation, *IEEE open journal of engineering in medicine and biology* 1 (2020) 108–115.

- [11] L. Wang, E. H. van Asseldonk, H. van der Kooij, Model predictive control-based gait pattern generation for wearable exoskeletons, in: *IEEE International conference on rehabilitation robotics*, 2011, pp. 1–6.
- [12] S. Zarandi, S. Sani, M. Tootoonchi, et al., Design and implementation of a real-time nonlinear model predictive controller for a lower limb exoskeleton with input saturation, *Iranian Journal of Science and Technology, Transactions of Electrical Engineering* 45 (1) (2021) 309–320.
- [13] O. Ulkir, G. Akgun, A. Nasab, et al., Data-driven predictive control of a pneumatic ankle foot orthosis, *Advances in Electrical and Computer Engineering* 21 (1) (2021) 65–74.
- [14] I. Jammeli, A. Chemori, H. Moon, S. Elloumi, S. Mohammed, An assistive explicit model predictive control framework for a knee rehabilitation exoskeleton, *IEEE/ASME Transactions on Mechatronics* (2021).
- [15] B. DeBoer, A. Hosseini, C. Rossa, A discrete non-linear series elastic actuator for active ankle-foot orthoses, *IEEE Robotics and Automation Letters* 7 (3) (2022) 6211–6217.
- [16] Y. Nakagaki, G. Zhai, A study on optimization algorithms in MPC, in: *Journal of Physics: Conference Series*, Vol. 1490, IOP Publishing, 2020, p. 012073.
- [17] M. Diehl, R. Findeisen, F. Allgöwer, et al., Nominal stability of real-time iteration scheme for nonlinear model predictive control, *IEE Proceedings-Control Theory and Applications* 152 (3) (2005) 296–308.
- [18] A. Steinboeck, M. Guay, A. Kugi, A design technique for fast sampled-data nonlinear model predictive control with convergence and stability results, *International Journal of Control* 93 (1) (2020) 81–97.
- [19] J. Han, From pid to active disturbance rejection control, *IEEE transactions on Industrial Electronics* 56 (3) (2009) 900–906.
- [20] B. DeBoon, S. Nokleby, C. Rossa, Multi-objective gain optimizer for a multi-input active disturbance rejection controller: Application to series elastic actuators, *Control Engineering Practice* 109 (2021) 104733.
- [21] S.-Y. Kuo, C.-H. Wu, C.-C. Chen, et al., A novel metaheuristic: Fast jaguar algorithm, in: *IEEE International Conference on Systems, Man, and Cybernetics (SMC)*, 2021, pp. 146–151.